The Origin of Stationary Planetary Waves in the Upper Mesosphere

ANNE K. SMITH

Atmospheric Chemistry Division, National Center for Atmospheric Research, Boulder, Colorado

(Manuscript received 7 April 2003, in final form 22 July 2003)

ABSTRACT

Satellite observations indicate that quasi-stationary planetary waves often exist to at least 100 km in the winter mesosphere. Waves are also seen in the summer upper mesosphere. A three-dimensional numerical model was used to simulate these waves and to diagnose the physical processes involved. The waves simulated in the model closely resemble observed waves. Several model runs that isolate specific processes are used to determine the relative importance of two forcing mechanisms. In the model, planetary waves that propagate from below are significantly damped at the altitude where gravity wave drag becomes large (about 75 km in the winter midlatitudes) or below if a reversal in the mean wind is encountered. Momentum forcing associated with breaking gravity waves that have been filtered by planetary-scale wind variations below acts to generate planetary waves in the middle and upper mesosphere. The amplitude from in situ forcing by gravity wave breaking exceeds the amplitude from the upward-propagating Rossby wave above 80 km.

1. Introduction

Quasi-stationary planetary-scale waves are a dominant feature of the winter middle atmosphere. The magnitude and variability of these waves in the stratosphere have been characterized from decades of radiosonde and more recently satellite observations. A body of theory, beginning with the classic study of Charney and Drazin (1966), has been able to explain most features of the observed waves in the stratosphere.

A smaller body of satellite observations for the upper mesosphere has been built up that clearly shows that quasi-stationary waves are normally present there as well. The first global-scale observations in the mesosphere from the pressure modulated radiometer (PMR) indicated that planetary waves were common as high as 85 km in the winter midlatitudes (Hirota and Barnett 1977) and that they appear in the Tropics as well (Venne et al. 1988). The structure of the mesospheric waves is sometimes incompatible with the interpretation of Rossby wave propagation from below (Marks 1989; Lawrence and Randel 1996). The *Upper Atmosphere Research Satellite* (*UARS*) provided measurements of horizontal winds throughout the mesosphere and lower thermosphere. Smith (1996, 1997) analyzed wintertime winds from the high resolution Doppler imager (HRDI); Wang et al. (2000) did a similar analysis on winds during all seasons measured by the wind imaging interferometer (WINDII). Both datasets indicate that waves are present throughout the winter mesosphere. The Cryogenic Infrared Spectrometer and Telescope for the Atmosphere (CRISTA) temperature data also indicate the presence of planetary waves (Offermann et al. 2003). Waves can also be inferred from other types of data. For example, Zaragoza et al. (2001) found high-latitude wave patterns in the OH nightglow near solstices. The nightglow is emitted at an altitude of about 87 km and is sensitive to advective and diffusive transport.

The behavior of stationary waves in the upper mesosphere has been difficult to characterize because of the need to separate stationary signals from the ubiquitous and variable atmospheric tides and the intermittent but sometimes large traveling planetary waves. It has proved straightforward to distinguish planetary waves from the migrating tides, that is, those that follow the apparent motion of the sun, in satellite datasets. The nonmigrating tides can be eliminated in a precessing satellite data set with 24-h sampling (Oberheide and Gusev 2002). Increasing evidence for the importance of nonmigrating tides (e.g., Hagan and Forbes 2002) indicates that upper-mesospheric wave observations from nonprecessing sources should be treated with great caution.

From the data that has been analyzed up to now, certain aspects of mesospheric planetary waves are well supported.

- Quasi-stationary planetary waves occur up to the mesopause (100 km) in midlatitudes of the winter hemisphere.
- It is commonly the case that Eliassen–Palm (EP) flux-

Corresponding author address: Dr. Anne K. Smith, Atmospheric Chemistry Division, National Center for Atmospheric Research, P.O. Box 3000, Boulder, CO 80307.
E-mail: aksmith@ucar.edu

es or other wave diagnostics do not support the interpretation that the waves propagate from below (Marks 1989; Smith 1997).
- There is a strong correlation, which can be positive or negative depending on altitude and other conditions, between the planetary-scale perturbations in the upper mesosphere and those in the stratosphere (Smith 1996, 1997; Wang et al. 2000).
- Stationary waves can have a significant presence in the Tropics and summer hemisphere (Venne et al. 1988; Wang et al. 2000; Smith 1999).

There are two mechanisms that are likely candidates for the presence of the waves in the winter hemisphere: 1) the Rossby waves that dominate in the stratosphere propagate vertically into the upper mesosphere, or 2) the upper-mesospheric planetary waves are generated in situ by breaking or dissipation of gravity waves having a zonally asymmetric upward flux. Both of these are consistent with the observed strong correlations between stratospheric and mesospheric wind perturbations. The correlation in the first case is because a propagating wave will have a westward phase shift in the vertical, leading to alternating negative and positive correlations at intervals of half the vertical wavelength. In the latter case, the strong wind variations normally seen in the winter stratosphere will filter gravity waves and can induce substantial longitudinal asymmetries in the upward flux of gravity waves (Holton 1984). The dissipation of those waves imparts a momentum forcing in the opposite direction to the winds that were responsible for the filtering. Analysis of the observations presented by Smith (1997) indicated that both mechanisms operate; which is dominant depends on how high into the middle atmosphere conditions are favorable for vertical Rossby wave propagation.

Also note that barotropic or baroclinic instability may be responsible for the generation and initial growth of planetary-scale waves in the summer hemisphere (e.g., Plumb 1983). The waves associated with this mechanism are traveling; the two periods that are most consistently observed are 2 days and 5 days. Because of the short periods, these are unlikely to be confused with the quasi-stationary waves discussed in this paper.

The studies cited above present very strong evidence for the frequent occurrence of quasi-stationary planetary waves in the upper mesosphere. The present paper uses a three-dimensional model to simulate the global structure of upper-mesospheric waves. The model simulations agree very well with the observational record. Various tests with the model are then used to obtain an assessment of the relative roles of propagation and in situ generation. The relationship between the waves in the winter and summer hemispheres is clarified.

The model indicates that planetary Rossby waves propagate to quite high altitudes. There is often a maximum in wave amplitude in the stratosphere. However, there is significant amplitude up to the point of the zonal wind reversal, which in these simulations usually occurs between 80 and 100 km and varies with latitude and time. The simulations indicate that gravity wave drag affects the structure of the planetary wave at all altitudes above the middle mesosphere. The initial effect is for the gravity wave drag to damp the planetary wave, and is primarily a result of the dependence of the gravity wave drag on the wind speed. However, at higher altitudes and most notably above the point of reversal of the background zonal wind, the gravity wave drag itself introduces an asymmetry. This can modify the amplitude or structure of the planetary wave or can generate a planetary wave where none is existing. The model simulations indicate that this in situ generation is responsible for the bulk of the planetary wave amplitude above about 85–90 km.

2. Model

The numerical model used in this study is a dynamics-only version of the new ROSE model. This is similar to that used in Smith and Ortland (2001), except that the vertical domain has been extended upward. The model solves the three-dimensional primitive equations on a sphere as a function of time. The model dynamics uses a leapfrog scheme on a grid; the current resolution includes 36 points in latitude (5°), 32 in longitude (11.25°), and 64 vertical levels.

In this version of the model, the upper boundary has been extended well into the thermosphere to avoid upper-boundary effects for tides and other waves. The vertical resolution is 0.3 scale heights (approximately 2.1 km in the middle atmosphere). The model domain extends from the tropopause to 21 scale heights, which corresponds to a geometric altitude of about 188 km. There is a sponge layer introduced gradually above 130 km to further reduce boundary impacts on the waves.

The physical parameters important in the model dynamics are diabatic heating and subgrid-scale processes. The radiative forcing uses the three-dimensional model computed temperature and density, but specifies the mixing ratios of the radiatively active gases (O_3, O_2, O, H_2O, and CO_2). Concentrations are based on the Committee on Space Research (COSPAR) International Reference Atmosphere (CIRA) reference ozone (Keating and Pitts 1987), the Mass Spectrometer, Incoherent Scatter (MSIS) empirical model (Hedin 1991), and CRISTA observations (Kaufmann et al. 2002), and if necessary are extended into the mesosphere and thermosphere using model calculations (Brasseur et al. 2000). The ultraviolet heating and infrared cooling are solved using the algorithm of Zhu (1994), which accounts for nonlocal thermodynamic equilibrium. The radiative heating and cooling are time dependent and contribute to the generation of realistic tides in the model. Diurnal average chemical heating is specified based on calculations from the model of Brasseur et al. (2000).

The most important of the subgrid processes is the

propagation, breaking, and dissipation of gravity waves. Momentum deposition by a spectrum of waves is represented using the algorithm developed by Hines (1997a,b). The adjustable parameters in the parameterization are similar to those determined by Akmaev (2001). The effect of stationary topographically forced gravity waves is included using a parameterization based on Lindzen (1981). The bottom of the parameterizations (the altitude from which gravity waves are launched) is in the upper troposphere at 200 hPa. Propagation and breaking are then determined by the vertical structure of instantaneous horizontal winds and static stability at each gridpoint. Momentum fluxes in the zonal and meridional directions are included. The parameterization does not account for refraction of gravity waves in the horizontal, which could be significant in some cases (Dunkerton and Butchart 1984).

The lower boundary conditions on horizontal winds, temperature, and geopotential change with each time step. The daily mean values are adapted from National Centers for Environmental Prediction (NCEP) analysis data beginning in 1991 and continuing into 1992. These have been smoothed in time and filtered to include only zonal mean and wavenumbers 1 and 2. Amplitude and phases of the diurnal and semidiurnal tides at the lower boundary are taken from the global-scale wave model (Hagan et al. 1999) for the appropriate time of year. Upper-boundary conditions are monthly diurnal means derived from the MSIS model (Hedin 1991).

Vertical diffusion includes contributions from three processes. A Richardson-number-dependent vertical diffusion coefficient adapted from that described by Williamson et al. (1987) is applied to horizontal momentum and potential temperature. Diffusion due to breaking gravity waves is a product of the gravity wave parameterization and is the dominant diffusive mechanism in the upper mesosphere. Molecular thermal diffusion is included with the parameterization of Banks and Kockarts (1973). Horizontal diffusion is provided by the filter described by Shapiro (1971). There is, in addition, a truncation of zonal wavenumbers greater than two at the latitudes nearest the poles ($\pm 87.5°$).

All of the model runs described here were begun in the middle of September and run through the end of the following April.

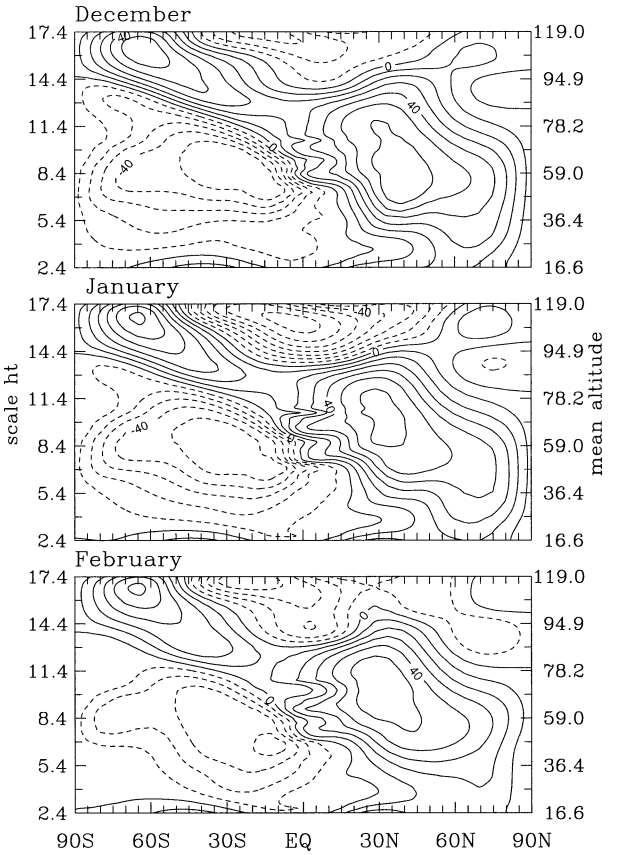

FIG. 1. Zonal mean wind simulated by the ROSE model averaged for the months of Dec–Feb. The contour interval is 10 m s^{-1}.

3. Simulated planetary waves

This section describes the planetary wave structure from the basic model run. Since the structure and propagation of Rossby waves depend strongly on the background zonal wind, we first need to verify that the model wind is realistic. Figure 1 shows the zonal mean wind as a function of latitude and scale height for the months of December, January, and February. The model simulations compare well with the *UARS* reference atmosphere zonal wind, based mainly on HRDI observations. Note, in particular, 1) the altitude of the reversal of the wintertime westerlies ranges from 80 to 95 km or even higher near the winter pole and 2) the continuous band of westerly winds extends from the winter hemisphere into the upper mesosphere of the summer hemisphere. A closer look at HRDI data for individual years (not shown) indicates that this cross-equatorial westerly band is present most months during the observed winters. The band of westerly winds across the equator is weaker and shallower in the *UARS* data than in the CIRA climatological winds; model winds agree better with the *UARS* data.

The wave fields that are considered in this paper are the dominant perturbation in model data that has been averaged over 24 h to remove all tidal contributions. Figure 2 shows a time series of the daily planetary wavenumber-1 geopotential height amplitude as a function of altitude at two latitudes: one in the Northern Hemisphere and one in the Southern Hemisphere. The large fluctuating planetary waves in the winter stratosphere (top) are clearly evident. The stratospheric maximum amplitudes occur around 50 km. There is then a minimum amplitude at about 80 km, and above there, another maximum in the amplitude at the mesopause (around 100 km). The time variation of the mesopause amplitude closely follows that in the stratosphere. The amplitude

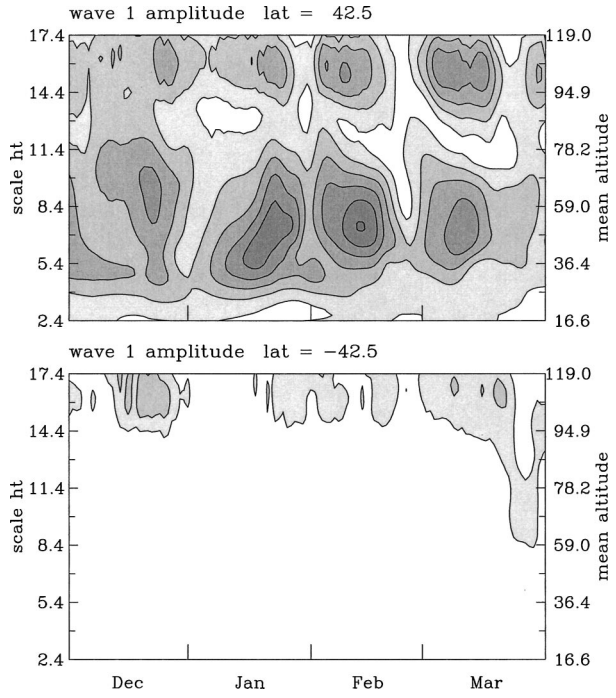

FIG. 2. Time series of the wavenumber-1 geopotential height amplitude as a function of scale height in midlatitudes of the Northern and Southern Hemispheres. The diurnal variations have been removed. The contour interval is 125 m.

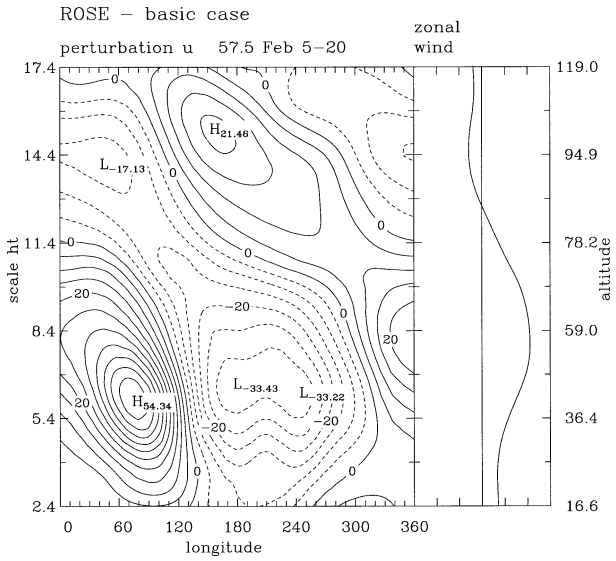

FIG. 3. (left) The longitude–altitude cross section of the perturbation zonal wind at 57.5°N averaged over the period 5–20 Feb. (right) The profile of the zonal mean wind for this period and latitude. The wind scale extends from −60 to 60 m s^{-1}; the vertical line indicates zero wind.

of the wave at the mesopause increases during the winter until, by March, it is larger than that in the stratosphere. The corresponding maximum amplitudes at 95–100 km are 40 m s^{-1} for zonal wind and 10 K for temperature.

In the summer hemisphere (bottom), there are no significant planetary waves in the stratosphere. There are waves in the mesopause region with amplitudes smaller than those seen in the winter mesopause region. The time scale for amplitude variations in the summer hemisphere waves is similar to that in the winter hemisphere, but the phase relationship is irregular.

a. Waves in the winter hemisphere

The wave structure during the large-amplitude event of early February will be examined in more detail. For ease of comparison with *UARS* observations, horizontal wind perturbations are emphasized. Figure 3 shows a longitude and altitude cross section of the time-mean perturbation zonal wind through the middle atmosphere at winter midlatitudes. The period in early February was characterized by large wavenumber-1 amplitude (see Fig. 2). The curve at the right shows the zonal mean wind for this latitude. The westward tilt with height of the perturbation wind is characteristic of a Rossby wave. In this case, the wave field is dominated by a zonal wavenumber 1. The largest perturbation winds are seen in the upper stratosphere. There is a minimum in the perturbation wind in the upper mesosphere, just below the altitude where the zonal mean wind reverses direction, and then a second region of high amplitude above the wind reversal. This type of pattern is seen throughout the winter in the model results.

The positions of the wind perturbations near the mesopause coincide with large amplitude perturbations in the stratosphere, but the signs are reversed. This is a similar feature to that found in observational winds, which led to the interpretation that asymmetries in the filtering of gravity waves in the stratosphere was responsible for the large mesopause wave signal. Figure 4 (top) shows the longitudinal distribution of gravity wave momentum driving associated with the results in Fig. 3. Gravity wave drag responds to the local wind and to the winds in all atmospheric layers between the tropopause and the level in question. It is evident from the figure that there are strong longitudinal asymmetries in the wave drag. Zones of negative momentum forcing near the altitude of the zonal wind reversal (75–80 km) are much stronger in the longitudes with perturbation westerly winds. At this altitude, the gravity wave drag not only causes a net momentum forcing that contributes to the reversal of the mean wind, but also contributes directly to the damping of the planetary wave.

Figure 4 (bottom) shows the ranges of zonal wind speed encountered in a vertical layer between the tropopause and the altitude of the upper mesospheric mean zonal wind reversal. As is typical for the winter midlatitudes, the wind directions are predominantly westerly and the speeds vary greatly with longitude. A broad range of westerly winds indicates that eastward gravity waves with a broad range of phase speeds are strongly filtered, and therefore that dissipation of surviving grav-

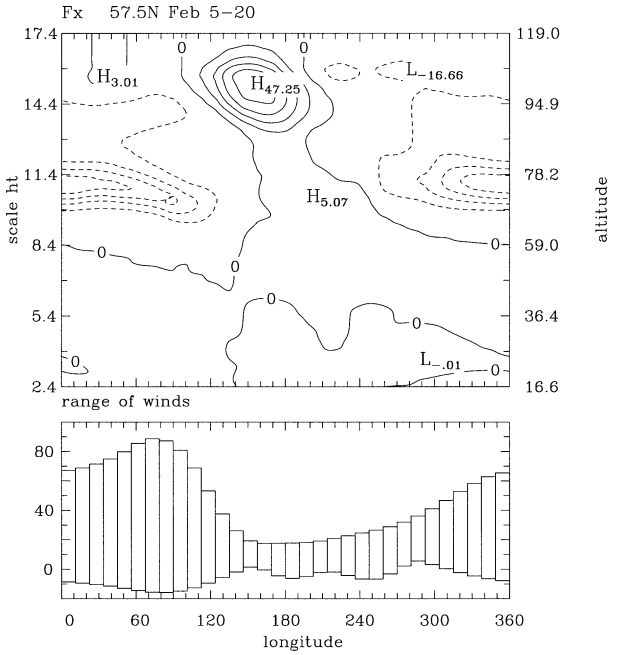

FIG. 4. (top) A longitude–altitude cross section of the net momentum forcing from parameterized gravity wave drag for the latitude and time shown in Fig. 3. Contour intervals are 10 m s^{-1} day^{-1}. (bottom) The range of zonal wind speeds encountered in a vertical column from the tropopause to the altitude of the mean zonal wind reversal.

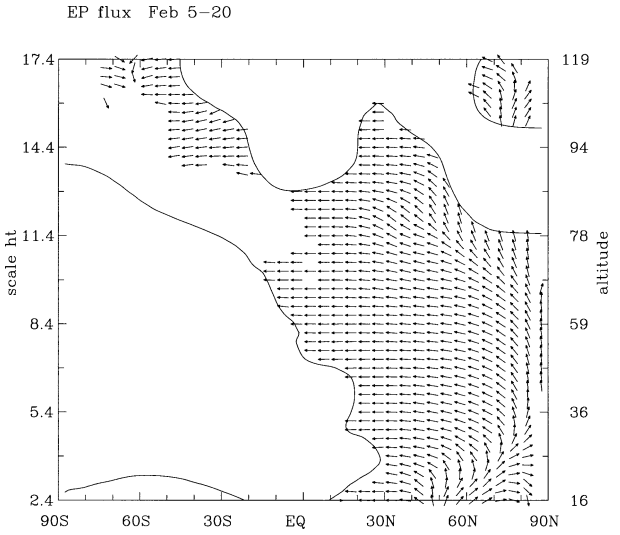

FIG. 5. The direction of EP flux whose amplitude exceeds the threshold value of 1% of the maximum. The heavy solid lines indicate zero mean zonal wind; EP flux arrows are shown only where the mean zonal wind is positive.

ity waves will give a westward (easterly) momentum forcing. A small range of winds indicates little filtering, and the net momentum flux from breaking gravity waves will be small. Note that in the model gravity wave parameterization, the source of gravity waves at the lower boundary is isotropic. The middle-atmosphere gravity wave drag depends not just on the upward flux but also on the local winds, which, as seen in Fig. 3, also vary with longitude. Model experiments discussed in section 4 will sort out these two effects.

A very useful diagnostic of Rossby wave propagation is the EP flux. Figure 5 shows the wavenumber-1 EP flux for the period illustrated in the Figs. 3 and 4. The contour lines delineate the regions of westerly wind. Eliassen–Palm flux vectors are shown with magnitude only, with a lower limit of 2% of the maximum value. Vectors are not shown for regions with easterly mean wind. In the stratosphere, the planetary wave propagates upward and equatorward. There is a clear indication of vertical propagation into the upper mesosphere in high latitudes. Vectors also indicate that lower-latitude wave propagation is equatorward in the winter hemisphere and that waves propagate across the equator in the westerly waveguide.

b. Waves in the Tropics and summer hemisphere

One very interesting finding from the observational analysis of Wang et al. (2000) was that there are quasi-stationary planetary waves in the summer hemisphere as well. The same phenomenon occurs in the ROSE model simulation. The EP flux diagram in Fig. 5 indicated the possibility of propagation across the equator in the band of westerly winds around 80–90 km.

Figure 6 shows a longitude by altitude cross section of the perturbation wind at 42.5°S, for comparison with Fig. 3. The perturbations in the Southern Hemisphere are smaller in magnitude and are confined to the highest part of the middle atmosphere. This is in contrast to the

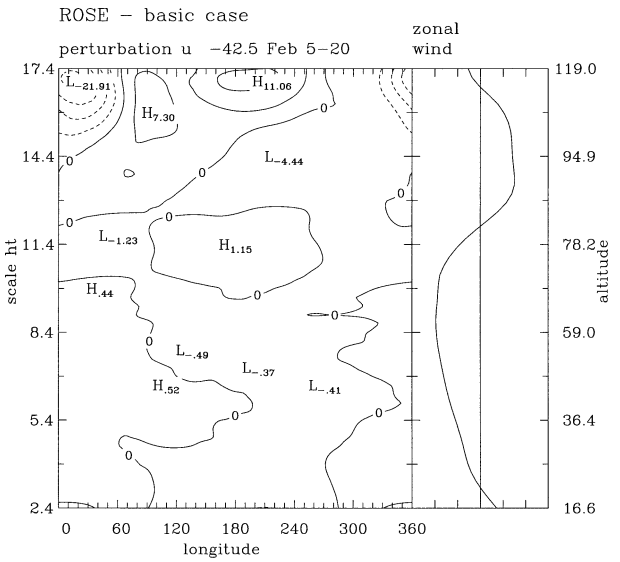

FIG. 6. (left) The longitude–altitude cross section of the perturbation zonal wind at 42.5°S averaged over the period 5–20 Feb. (right) The profile of the zonal mean wind for this period and latitude. The scale is as in Fig. 3.

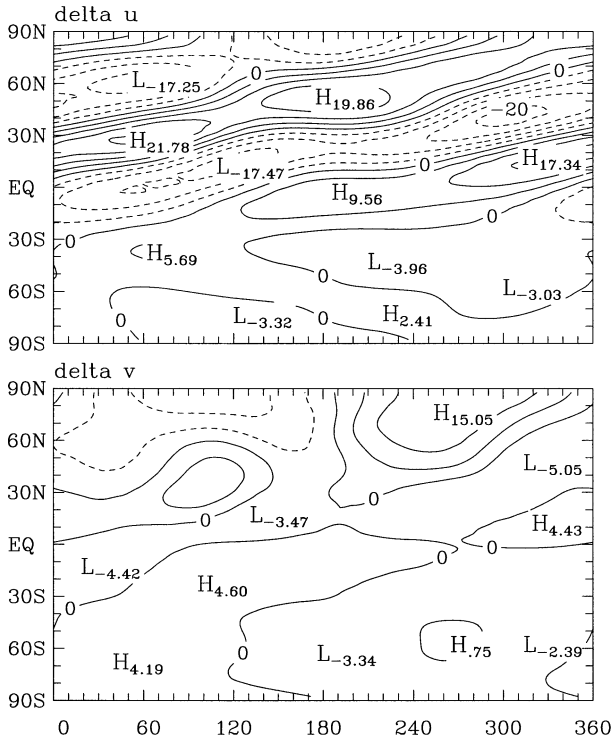

FIG. 7. Perturbation (top) zonal and (bottom) meridional wind as a function of latitude and longitude for the period 5–20 Feb at about 92 km. Contour interval is 5 m s^{-1}.

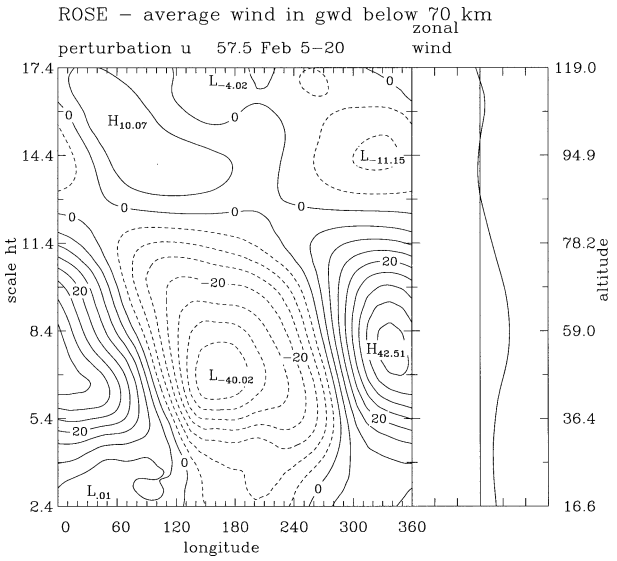

FIG. 8. As in Fig. 3, but for a model run in which zonal wind perturbations below 70 km were suppressed in the gravity wave drag parameterization.

observations of Wang et al. (2000), who found that zonal wind amplitudes in the summer hemisphere were as large as or larger than those in the winter. The discrepancy may be because the model does not consider zonal asymmetries in the gravity wave flux emerging from the troposphere (Osprey and Lawrence 2001).

Figure 7 shows the perturbation zonal and meridional wind at 92 km for this period. This altitude is just at the upper edge of the cross-equatorial waveguide in the mean wind for February (Fig. 1). The zonal wind structure is wavelike in latitude extending throughout the winter hemisphere and across the equator to about 30°S. The wave pattern looks very much like a Rossby wave, with an eastward tilt with latitude. The meridional wind structure is also wavelike and has a similar meridional wavelength. The amplitude is much smaller than that of the zonal wind. The EP fluxes for this period and altitude are consistent with wave propagation toward the south.

4. Model experiments to determine the generation of upper-mesospheric planetary waves

The model experiments are designed to address several questions regarding the origin and propagation of the mesospheric planetary waves.

First we examine the mechanism identified by Smith (1996) that longitudinal asymmetries in gravity wave momentum forcing associated with breaking or other dissipation generates planetary waves in situ in the upper mesosphere. The gravity wave flux at any particular level departs from zonal symmetry due to two factors: filtering of the wave spectrum by planetary-scale wind variations in the layers below or variations in the wave source in the troposphere. The strong correlation between stratospheric and upper-mesospheric planetary waves suggests that the former is dominant. Because the ROSE model does not resolve the troposphere, we will not address the latter mechanism. The gravity wave drag depends on the flux of wave activity from below but also quite strongly on the ambient conditions.

The model experiments to investigate the role of filtering of the gravity wave spectrum work from both directions: looking at the planetary wave structure when the longitudinal variability of gravity waves is suppressed, and looking at the planetary wave structure when the propagating Rossby waves are suppressed but the asymmetries in gravity wave drag are retained.

a. Model experiment: Suppression of gravity wave filtering in the stratosphere

Stratospheric filtering of gravity waves can be suppressed by using zonally averaged zonal and meridional winds in the gravity wave drag calculation, up to a specified altitude. In this model case, the horizontal winds up to 70 km are zonally averaged before being used in the gravity wave parameterization. In the next few levels above 70 km, the winds return to the full model wind. Everything else in this model case is identical to the basic model run.

Figure 8 shows the results of this run, for comparison with Figs. 3 and 4 from the basic run. From Fig. 8 it

is seen that the planetary wave in the upper mesosphere still appears, but its amplitude is substantially reduced and its phase is shifted in longitude. Note, however, that the wave amplitude in the middle mesosphere (around 75 km) is stronger in this case than in the basic case. In this region, filtering by winds contributes to the gravity wave drag that normally damps the waves (Miyahara 1985, 1986). As one would expect, the longitudinal variations in momentum forcing due to gravity wave drag (not shown) are strongly curtailed in this case compared to the basic model integration.

As seen in Fig. 8, if the zonal wind perturbations below 70 km are suppressed, the planetary wave amplitude at 95 km decreases by about 50%. Additional tests with the model indicate that filtering is important through the middle mesosphere. When the zonal wind perturbations below 50 km are suppressed in the gravity wave drag parameterization, the amplitude above 80 km is intermediate between that seen in Figs. 3 and 8. However, suppressing longitudinal variations in the background wind up to 90 km gives results that are very similar to those shown in Fig. 8.

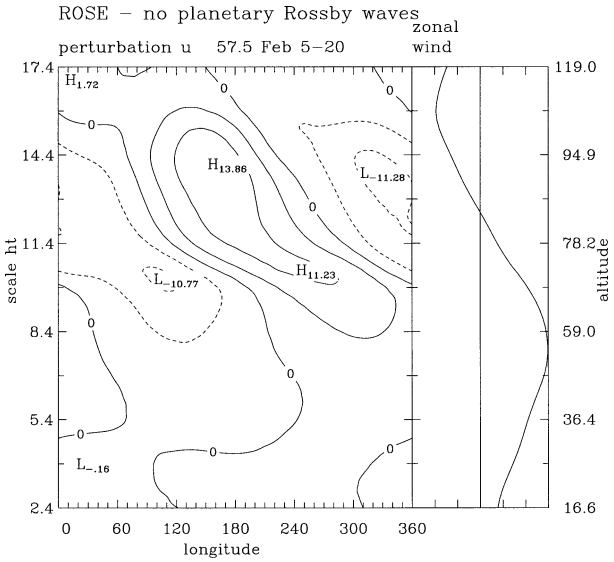

FIG. 9. As in Fig. 3, but for a model run in which no planetary waves were forced at the lower boundary, but the longitudinal variations in gravity wave drag from the basic run were included.

b. Model experiment: Suppression of propagating Rossby wave

In the next experiment, the lower boundary of the model is modified so that no planetary waves are forced. If this is done with no other model changes, quasi-stationary planetary waves do not appear at all in the model. To test to what extent waves in the basic run are generated by the zonal asymmetries in gravity wave drag, we save and add that drag into this run. This is done in the following way. In the basic model run, the gravity wave drag for each time step during a day is averaged to give the mean value for the day. Then the zonal mean is removed; the remaining gravity wave drag is that part associated with planetary-scale disturbances. The model is then return, but with zonally symmetric conditions at the lower boundary, so that no planetary waves propagate into the middle atmosphere from below. The perturbation gravity wave drag is imposed; other components of the drag (in response to the zonal mean winds and tides) are generated as normal. In this run, the only source of planetary waves is gravity wave drag within the middle atmosphere. Once planetary waves are generated by asymmetries in the drag, they can then propagate vertically if the conditions are suitable.

Figure 9 shows a longitude–altitude cross section for this case, which can be compared to Fig. 3. Planetary waves appear in the middle and upper mesosphere and follow the vertical tilt of the original planetary wave. In this model case, the zonal wind is substantially different due to the absence of Rossby waves in the stratosphere. The reversal in the zonal wind occurs at a lower altitude because the zonal mean gravity wave drag is significantly stronger. In this model run, the waves that are generated by gravity wave drag have their maximum amplitude just above the level of zero zonal mean wind. The EP fluxes and flux divergences (not shown) are very small, indicating that propagation of the induced disturbances does not play a significant role.

Figure 10 compares the time evolution of wavenumber-1 geopotential amplitudes propagating from below (as shown in Fig. 8) and generated from gravity wave drag (as shown in Fig. 9) at 57°N. Propagating planetary waves dominate in the lower mesosphere; gravity-wave-generated planetary waves dominate near the mesopause. During much of the winter, the transition from propagating to gravity-wave-generated waves occurs around 80 km. The highest altitude shown (85 km) has more irregularity; either propagating or in situ forced waves can dominate the wave field.

5. Conclusions

A three-dimensional model is used to investigate the mechanism for generation of stationary planetary waves at the mesopause. The model simulates waves that resemble the wave patterns that have been seen in satellite wind and geopotential observations. Model experiments probe the contributions to the waves from vertical propagation of Rossby waves from the stratosphere and from in situ generation within the mesosphere by gravity wave drag.

The model zonally averaged winds are westerly throughout most of the middle atmosphere in the winter hemisphere. The wind reversal varies with latitude and tends to occur between 75 and 95 km. Rossby wave propagation is allowed throughout this depth. The propagating waves are increasingly damped by gravity wave

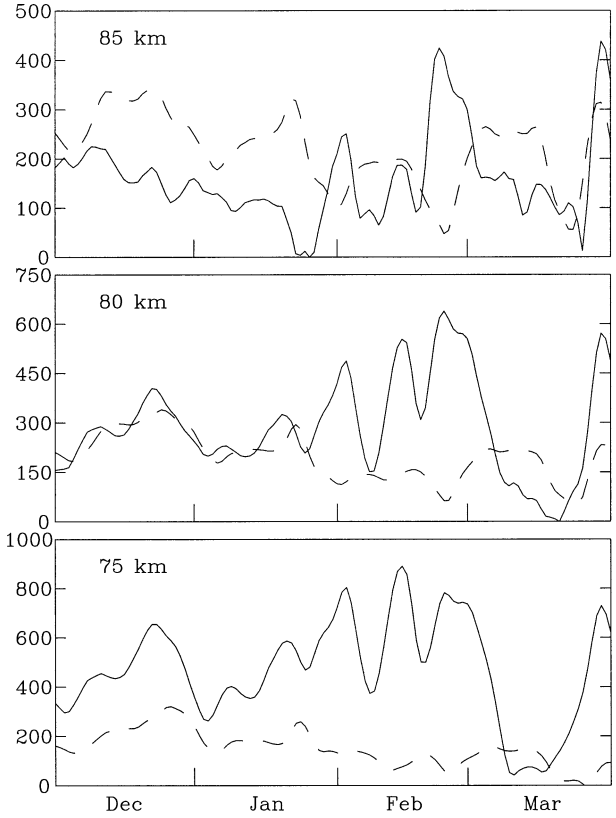

FIG. 10. Time series of wavenumber-1 geopotential height amplitude at 57.5°N at three altitudes. The dashed line is the wave generated by gravity wave drag; the solid is the upward-propagating Rossby wave. Note the difference in the axes.

drag in the mesosphere and are significantly diminished above the zero wind line if the upward flux of gravity waves is constrained to be zonally symmetric.

The upward flux of propagating gravity waves from the troposphere develops large-scale perturbations in longitude due to filtering by middle-atmosphere winds. According to theory and simulated in the Hines gravity wave drag parameterization, this filtering affects the momentum forcing to the background flow when the waves break or dissipate. The planetary-scale perturbations to the horizontal winds generated by this mechanism are largest just above the level of the mean zonal wind reversal.

Acknowledgments. Support for this work was provided by NASA Office of Space Science. The National Center for Atmospheric Research is operated by the University Corporation for Atmospheric Research under the sponsorship of the National Science Foundation.

REFERENCES

Akmaev, R., 2001: Simulation of large-scale dynamics in the mesosphere and lower thermosphere with the Doppler-spread parameterization of gravity waves. 1. Implementation and zonal mean climatologies. *J. Geophys. Res.*, **106,** 1193–1204.

Banks, P. M., and G. Kockarts, 1973: *Aeronomy*. Part B, Academy Press, 355 pp.

Brasseur, G. P., A. K. Smith, R. Khosravi, T. Huang, and S. Walters, 2000: Natural and human-induced perturbations in the middle atmosphere: A short tutorial. *Atmospheric Science across the Stratopause*, D. E. Siskind, S. D. Eckermann, and M. E. Summers, Eds., American Geophysical Union, 7–20.

Charney, J., and P. Drazin, 1961: Propagation of planetary-scale disturbances from the lower into the upper atmosphere. *J. Geophys. Res.*, **66,** 83–109.

Dunkerton, T. J., and N. Butchart, 1984: Propagation and selective transmission of gravity waves in a sudden warming. *J. Atmos. Sci.*, **41,** 1443–1460.

Hagan, M. E., and J. M. Forbes, 2002: Migrating and nonmigrating diurnal tides in the middle and upper atmosphere excited by tropospheric latent heat release. *J. Geophys. Res.*, **107,** 1062, doi:10.1029/2002JADD9466.

——, M. D. Burrage, J. M. Forbes, J. Hackney, W. J. Randel, and X. Zhang, 1999: GSWM-98: Results for migrating solar tides. *J. Geophys. Res.*, **104,** 6813–6827.

Hedin, A. E., 1991: Extension of the MSIS thermosphere model into the middle and lower atmosphere. *J. Geophys. Res.*, **96,** 1159–1172.

Hines, C. O., 1997a: Doppler spread parameterization of gravity wave momentum deposition in the middle atmosphere. 1. Basic formulation. *J. Atmos. Solar Terr. Phys.*, **59,** 371–386.

——, 1997b: Doppler spread parameterization of gravity wave momentum deposition in the middle atmosphere. 2. Broad and quasimonochromatic spectra and implementation. *J. Atmos. Solar Terr. Phys.*, **59,** 387–400.

Hirota, I., and J. Barnett, 1977: Planetary waves in the winter mesosphere—Preliminary analysis of *Nimbus 6* PMR results. *Quart. J. Roy. Meteor. Soc.*, **103,** 487–498.

Holton, J. R., 1984: The generation of mesospheric planetary waves by zonally asymmetric gravity wave breaking. *J. Atmos. Sci.*, **41,** 3427–3430.

Kaufmann, M., O. A. Gusev, K. U. Grossmann, R. G. Roble, M. E. Hagan, C. Hartsough, and A. A. Kutepov, 2002: The vertical and horizontal distribution of CO_2 densities in the upper mesosphere and lower thermosphere as measured by CRISTA. *J. Geophys. Res.*, **107,** 8182, doi:10.1029/2001JD000704.

Keating, G. M., and M. C. Pitts, 1987: Proposed reference models for ozone. *Adv. Space Res.*, **7,** 937–947.

Lawrence, B. N., and W. J. Randel, 1996: Variability in the mesosphere observed by the *Nimbus 6* pressure modulated radiometer. *J. Geophys. Res.*, **101,** 23 475–23 489.

Lindzen, R. S., 1981: Turbulence and stress owing to gravity wave and tidal breakdown. *J. Geophys. Res.*, **86,** 9707–9714.

Marks, C. J., 1989: Some features of the climatology of the middle atmosphere revealed by *Nimbus 5* and *6*. *J. Atmos. Sci.*, **46,** 2485–2508.

Miyahara, S., 1985: Suppression of stationary planetary waves by internal gravity waves in the mesosphere. *J. Atmos. Sci.*, **42,** 100–107.

——, Y. Hayashi, and J. D. Mahlman, 1986: Interactions between gravity waves and planetary-scale flows simulated by the GFDL ''SKYHI'' general circulation model. *J. Atmos. Sci.*, **43,** 1844–1861.

Oberheide, J., and O. A. Gusev, 2002: Observation of migrating and nonmigrating diurnal tides in the equatorial lower thermosphere. *Geophys. Res. Lett.*, **29,** 2167, doi:10.1029/2002GL016213.

Offermann, D., M. Donner, K. U. Grossman, O. Gusev, M. Jarisch, M. Kaufmann, J. Oberheide, and A. I. Semenov, 2003: Zonal asymmetries in middle atmosphere temperatures. *Adv. Space. Res.*, in press.

Osprey, S. M., and B. N. Lawrence, 2001: A possible mechanism for in situ forcing of planetary waves in the summer extratropical mesosphere. *Geophys. Res. Lett.*, **28,** 1183–1186.

Plumb, R. A., 1983: Baroclinic instability at the summer mesosphere:

A mechanism for the quasi-two-day wave? *J. Atmos. Sci.,* **40,** 262–270.

Shapiro, 1971: The use of linear filtering as a parameterization of atmospheric diffusion. *J. Atmos. Sci.,* **28,** 523–531.

Smith, A. K., 1996: Longitudinal variations in mesospheric winds: Evidence for gravity wave filtering by planetary waves. *J. Atmos. Sci.,* **53,** 1156–1173.

——, 1997: Stationary planetary waves in upper-mesospheric winds. *J. Atmos. Sci.,* **54,** 2129–2145.

——, 1999: Observations of low frequency Kelvin waves in the mesosphere. *Earth Planets Space,* **51,** 649–656.

——, and D. A. Ortland, 2001: Modeling and analysis of the structure and generation of the terdiurnal tide. *J. Atmos. Sci.,* **58,** 3116–3134.

Venne, D. E., D. G. Dartt, and C. D. Rodgers, 1988: A stationary planetary wave feature in the tropical mesopause temperature field. *Geophys. Res. Lett.,* **15,** 1129–1132.

Wang, D. Y., W. E. Ward, G. G. Shepherd, and D.-L. Wu, 2000: Stationary planetary waves inferred from WINDII wind data taken within the altitudes 90–120 km during 1991–96. *J. Atmos. Sci.,* **57,** 1906–1918.

Williamson, D. L., J. T. Kiehl, V. Ramanathan, R. E. Dickinson, and J. J. Hack, 1987: Description of NCAR Community Climate Model (CCM1). NCAR Tech. Note NCAR/TN-285+STR, 112 pp.

Zaragoza, G., F. W. Taylor, and M. Lopez-Puertas, 2001: Latitudinal and longitudinal behavior of the mesospheric OH nightglow layer as observed by the Improved Stratospheric and Mesospheric Sounder on UARS. *J. Geophys. Res.,* **106,** 8027–8033.

Zhu, X., 1994: An accurate and efficient radiative algorithm for middle atmosphere models. *J. Atmos. Sci.,* **51,** 3593–3614.